BioMACROMOLECULES

Article

pubs.acs.org/Biomac

Identification of Critical Surface Parameters Driving Lectin-Mediated Capture of Bacteria from Solutions

Mohammadali Masigol,[†] Niloufar Fattahi,[†] Niloy Barua,[†] Bradley S. Lokitz,[‡] Scott T. Retterer,[‡,§] Thomas G. Platt,[∥] and Ryan. R. Hansen*[,†]

[†]Chemical Engineering Department and [∥]Division of Biology, Kansas State University, Manhattan, Kansas 66506, United States

[‡]Center for Nanophase Materials Sciences and [§]Biosciences Division, Oak Ridge National Laboratory, Oak Ridge, Tennessee 37831, United States

Supporting Information

ABSTRACT: Lectin-functional interfaces are useful for isolation of bacteria from solutions because they are low-cost and allow nondestructive, reversible capture. This study provides a systematic investigation of physical and chemical surface parameters that influence bacteria capture over lectin-functionalized polymer interfaces and then applies these findings to construct surfaces with significantly enhanced bacteria capture. The designer block copolymer poly(glycidyl methacrylate)-*block*-poly(vinyldimethyl azlactone) was used as a lectin attachment layer, and lectin coupling into the polymer film through azlactone−lectin coupling reactions was first characterized. Here, experimental parameters including polymer areal chain density, lectin molecular weight, and lectin coupling buffer were systematically varied to identify parameters driving highest azlactone conversions and corresponding lectin surface densities. To introduce physical nanostructures into the attachment layer, nanopillar arrays (NPAs) of varied heights (300 and 2100 nm) were then used to provide an underlying surface template for the functional polymer layer. Capture of *Escherichia coli* on lectin−polymer surfaces coated over both flat and NPA surfaces was then investigated. For flat polymer interfaces, bacteria were detected on the surface after incubation at a solution concentration of 10^3 cfu/mL, and a corresponding detection limit of 1.7×10^3 cfu/mL was quantified. This detection limit was 1 order of magnitude lower than control lectin surfaces functionalized with standard, carbodiimide coupling chemistry. NPA surfaces containing 300 nm tall pillars further improved the detection limit to 2.1×10^2 cfu/mL, but also reduced the viability of captured cells. Finally, to investigate the impact of cell surface parameters on capture, we used *Agrobacterium tumefaciens* cells genetically modified to allow manipulation of exopolysaccharide adhesin production levels. Statistical analysis of surface capture levels revealed that lectin surface density was the primary factor driving capture, as opposed to exopolysaccharide adhesin expression. These findings emphasize the critical importance of the synthetic interface and the development of surfaces that combine high lectin densities with tailored physical features to drive high levels of capture. These insights will aid in design of biofunctional interfaces with physicochemical surface properties favorable for capture and isolation of bacteria cells from solutions.

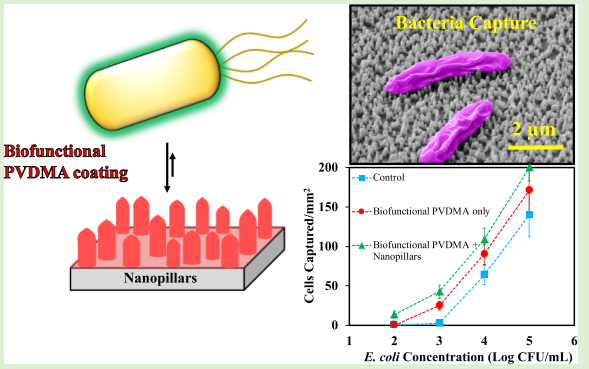

1. INTRODUCTION

Developing synthetic biological interfaces that enable reliable and rapid capture and enrichment of microorganisms is useful for applications in food and water monitoring, clinical diagnostics, applied medicine, and industrial and environmental monitoring.[1−3] Microbe capture and enrichment support rapid, culture-free detection and thus faster, more informed responses.[4,5] Although synthetic interfaces functionalized with antibodies targeting microbial surface antigens are most commonly used for capture,[6−8] carbohydrate recognition with lectin-functionalized interfaces has been increasingly considered as an alternative approach, as microorganisms express extracellular surface carbohydrates in the form of lipopolysaccharides, glycolipids, and glycoproteins.[2,5] Lectins have advanced glycomic research, as they can be used to understand the role of glycans in a variety of cellular processes.[9−11] With respect to cell capture, lectin interfaces have been used for isolating and enriching cancerous cells from whole blood,[12,13] bacterial pathogens from food and environmental samples,[14] and for removal of microbial pathogens from whole blood for sepsis therapy.[15] However, limitations in capture efficiency often arise because carbohydrate−protein interactions are inherently weaker than antibody−antigen interactions,[16,17] with equilibrium dissociation constants (K_D) higher by a factor of 10^2 to 10^3.[1] Thus, developing physicochemically tunable interfaces with improved control of lectin density, orientation, and stability is key for utilizing

Received: May 2, 2019
Published: May 31, 2019

DOI: 10.1021/acs.biomac.9b00609
Biomacromolecules XXXX, XXX, XXX−XXX

lectin−carbohydrate interactions for cell capture and other glycomic research applications.[18−20]

Synthetic, biofunctional polymers have been used to tune physicochemical and biological interface properties to improve cell capture and surface viability.[21,22] For example, polymer films containing reactive azlactone groups have been used to immobilize a suite of biomolecules (lectins, proteins, and peptides) through rapid coupling with amine or thiol groups.[23,24] Compared to other bioconjugation chemistries (e.g., EDC−NHS), the higher hydrolytic stability of azlactones, combined with one-step "click" reactions with biomolecules, makes it a robust route to biofunctionalization.[25,26] Azlactone-functionalized copolymers have been used to generate reliable platforms for cell culture investigations. For instance, Schmitt et al. presented a peptide-coupled interface using a triblock copolymer consisting of glycidyl methacrylate, polyethylene glycol, and azlactone-based polymers for human mesenchymal stem cell adhesion and growth. The polymer coatings generated a highly stable biointerface, allowing for long-term (>2 week) cell culture experiments.[24] Other amine-functionalized biomolecules can be coupled to polyvinyl dimethyl azlactone (PVDMA) surfaces as well. Broderick et al. presented a top-down fabrication method using poly(ethylamine)/PVDMA multilayer surfaces to generate patterned arrays of amine-terminated oligonucleotides for DNA hybridization studies. Azlactone-bearing background regions were passivated by treatment with D-glucamine to prevent nonspecific biomolecule adsorption.[27] Neri et al. used azlactone-bearing polymers to modulate the chemical properties of graphene. They generated the azlactone−graphene interface for the selective attachment of chemical and biological targets such as glutathione disulfide.[28]

In order to address limitations associated with lectin-binding, Hansen et al. applied the dually reactive block copolymer poly(glycidyl methacrylate)-*block*-poly(vinyl dimethyl azlactone) (PGMA-*b*-PVDMA) to generate three-dimensional, microscale patterns of lectins over surfaces for bacteria capture, and demonstrated that these polymer treatments could couple high lectin densities and capture significantly more bacteria from solutions compared to surfaces containing physisorbed lectins.[29,30] However, these polymer coatings were unoptimized, as lectin−polymer and lectin−cell interactions were not studied. In fact, few reports have provided a detailed understanding of how experimental parameters, such as pH or polymer surface density, affect biomolecule coupling in these systems.[31] The work presented here builds off the previous system,[29] and provides a fundamental understanding of the critical surface and coupling parameters that influence lectin−polymer functionalization over PVDMA-based coatings. In addition to these chemical parameters, physical surface features such as nanoscale architecture also impact capture by providing increased surface area for bacteria interaction.[32] For example, Friedlander et al. recently showed that submicron surface crevices increase *Escherichia coli*−surface adhesion by providing anchoring sites for flagella.[33] Given this premise, we used nanofabrication methods to generate nanopillar arrays (NPAs)[34] with controlled pillar heights to provide an interface with a tailored nanostructure. This allowed for further investigation on the impact of nanoscale surface features on a lectin-based capture in this system. The combination of favorable physical and chemical surface features was then used to construct surfaces providing improved gains in sensitivity and capture efficiency.

Finally, the effect of exopolysaccharide production levels on capture over these interfaces is investigated, which is important as capture is also influenced by surface properties of the bacterial cell, such as amount of extracellular polymeric substances present.[35] For these studies, *Agrobacterium tumefaciens* was selected as a model microbe as it can release a broad range of exopolysaccharides such as cellulose, succinoglycan, β-1,2 glucan, β-1,3 glucan, and unipolar polysaccharides (UPPs).[36,37] Prior research has established an *A. tumefaciens* strain whose UPP adhesin production can be experimentally manipulated in the absence of other exopolysaccharides.[37,38] This biological resource allowed for an experimental evaluation of the relative importance of lectin surface density and adhesin production to bacterial cell capture.

2. EXPERIMENTAL SECTION

2.1. Materials. Sodium carbonate (Na_2CO_3), sodium bicarbonate ($NaHCO_3$), 2-(*N*-morpholino)ethanesulfonic acid hemisodium salt (MES), 4-(2-hydroxyethyl)piperazine-1-ethanesulfonic acid (HEPES), manganese(II) chloride ($MnCl_2$), calcium chloride ($CaCl_2$), anhydrous toluene, 3-aminopropyl triethoxysilane (APTES), *N*-(3-dimethylaminopropyl)-*N*′-ethylcarbodiimide (EDC), *N*-hydroxysuccinimide (NHS), dimethylformamide (DMF), succinic anhydride (SA), triethylamine, isopropyl β-D-1-thiogalactopyranoside (IPTG), and glutaraldehyde solution (25 wt % in water) were purchased from Sigma-Aldrich. *Triticum vulgare* lectin (wheat germ agglutinin, WGA), *Helix pomatia* lectin (HPA), and concanavalin A from *Canavalia ensiformis* (ConA) were purchased from Sigma-Aldrich and diluted to specific concentrations in buffer and stored at −20 °C. WGA−FITC conjugate and HPA−Alexa Fluor 488 conjugate were purchased from Fisher Scientific, diluted to the desired concentration in 1× phosphate-buffered saline (PBS), and stored at −20 °C. 1× PBS buffer (pH 7.4), carbonate/bicarbonate buffer (pH 9.3, pH 10.0, and pH 10.4), HEPES buffer (pH 8.0), and MES buffer (pH 6.0) were made using standard recipes.[39] WGA and HPA were dissolved in the buffers with pH 7.4, 9.3, and 10.4. ConA was dissolved in the buffers with pH 6.0, 8.0, and 10.0 that contained 100 μM of $MnCl_2$ and $CaCl_2$ (Mn^{2+} and Ca^{2+} are critical for the carbohydrate interaction).[40] *E. coli* K12-mCherry and *A. tumefaciens* JX110 (Δ*crdS*Δ*cel*Δ*exoA*Δ*chvAB* mutant of strain C58) carrying pJW110 (encoding an IPTG-inducible P_{lac}-*pleD*) were stored in 25% glycerol stocks at −80 °C.[37,38] $PGMA_{56}$-*b*-$PVDMA_{175}$ was synthesized as reported by Lokitz et al.,[41] and stored at −20 °C until use. A LIVE/DEAD BacLight Bacterial Viability Kit was purchased from ThermoFisher Scientific and stored at −20 °C until use. Silicon (Si) wafers were purchased from WRS Materials.

2.2. Polymer Cross-Linking over Flat Si Substrates and Lectin Functionalization. Flat Si wafers (9 × 9 mm) were treated with oxygen plasma (3 min), then treated with Piranha solution (3:1 v/v H_2SO_4/30% H_2O_2 at 120 °C for 30 min) (**Caution**! strongly corrosive) for cleaning and to generate surface hydroxyl groups to be reacted with the epoxy group existing in the PGMA block.[42] The wafers were then washed with ultrapure water and used within 24 h of cleaning. The $PGMA_{56}$-*b*-$PVDMA_{175}$ polymer was dissolved in anhydrous chloroform at the specified concentration. The solution (100 μL) was spin-coated over wafers (1500 rpm, 15 s), and substrates were then placed in a vacuum oven for 18 h (annealing temperature: 110 °C). Cross-linking of the PGMA epoxy groups to the surface hydroxyl groups allowed for covalent attachment to the Si substrate.[41] After annealing, acetone was used to sonicate the polymer-coated surfaces for 10 min to remove physisorbed polymer. The substrates were dried with N_2 and stored at vacuum condition until further use. Using the ellipsometry data, the areal chain density has been calculated using the following equation[41,42]

$$\sigma = \frac{h\rho N_a}{M_n} \quad (1)$$

DOI: 10.1021/acs.biomac.9b00609
Biomacromolecules XXXX, XXX, XXX−XXX

In this equation, h corresponds to polymer film thickness (nm), ρ is the density of the block co-polymer (g/cm^3), N_a and M_n represent Avogadro's number and polymer molecular weight (34 231 g/mol), respectively. Lectin functionalization to the PVDMA chains (Scheme S1A) was conducted by incubating solutions of WGA, HPA, or ConA in their appropriate buffers over azlactone-functionalized substrates for 1 h. Substrates were incubated in 100 μL volumes at 0.1 mg/mL lectin concentrations unless otherwise noted. A 0.05% solution of Tween 20 in appropriate buffer was used to wash the substrates. Identical protocols were followed for functionalization over polymer-coated nanopillar surfaces from Section 2.3.

2.3. Fabrication of NPA Surfaces. NPA surfaces were created using a combination of mask-less reactive ion etching (RIE) and plasma-enhanced chemical vapor deposition (PECVD). Clean 4″ ⟨100⟩ silicon wafers were etched in an Oxford Plasmalab 100 RIE system (Oxford Instruments, Concord, MA) for the desired time (3.3 or 10.3 min) using a "black silicon"[43] etch recipe (100 W dc bias, 1000 W ICP RF power, 20 °C, 35 mT, 65 sccm SF_6, 45 sccm O_2). This etch process simultaneously generates random SiO_2 micromasks across the sample surface while removing exposed silicon, creating nanopillar texturing. A thin (∼32 nm) layer of SiO_2 was then deposited on the samples via PECVD to provide an oxide attachment layer for the $PGMA_{56}$-*b*-$PVDMA_{175}$ polymer. Samples were placed in an Oxford Plasmalab 100 PECVD system (Oxford Instruments, Concord, MA) and coated with SiO_2 at approximately 1.1 nm/min for 30 s (350 °C, 1000 mT, 20 W RF power, 170 sccm 5% silane in Ar, 170 sccm N_2O). Samples were imaged in an FEI NovaLab Dual Beam system prior to being coated with SiO_2. Coating of $PGMA_{56}$-*b*-$PVDMA_{175}$ on samples was performed according to the procedure described in Section 2.2. Polymer-coated nanopillar surfaces are referenced according to their pillar dimensions as low aspect ratio NPA (LAR-NPA) and high aspect ratio NPA (HAR-NPA).

2.4. Preparation of Bacterial Samples and Capture Conditions. Liquid cultures were prepared by inoculating a single colony of *E. coli* K12-mCherry in 3 mL of LB media (37 °C, 215 rpm). Bacteria were harvested by centrifugation, washed and re-suspended in 1× PBS solution. *E. coli*-mCherry solution with desired optical density OD) was incubated over the lectin-functionalized substrates by gentle rocking. After incubation of 1 mL of microbe solution for 1 h, the substrates were immersed in 1× PBS buffer (0.05% Tween 20) to remove unattached bacteria followed by fixing the attached cells using 2.5% glutaraldehyde in ultrapure water. The substrates were then washed using ultrapure water and dried by aspirating water off the surface. Bacteria concentration in solution was quantified using OD (OD_{600}) measurements. *A. tumefaciens* was cultured in AT minimal media supplemented with 0.5% glucose (w/v), 15 mM $(NH_4)_2SO_4$, and 100 mg/mL gentamicin.[44,45] For each culture a single colony of *A. tumefaciens* JX110 pJW110 was inoculated into 2 mL of media and cultured for 22−24 h (28 °C, 215 rpm). We then used 10 μL of this culture to inoculate 2 mL of fresh media supplemented with either 0, 50, 100, 200, or 400 μM IPTG. These cultures grew for an additional 10−14 h such that log phase cultures could be used for subsequent experiments. A growth curve verified that these cells were taken in the log phase after this amount of time (Figure S1).

2.5. Lectin Binding Assay. The UPP production by *A. tumefaciens* JX110 pJW110 was visualized by using WGA labeled with FITC.[37] The washed cell solution (1.0 mL) was incubated with 10 μg/mL solutions of WGA−FITC (1.0 mg/mL) for 1.5 h at 25 °C while shaking at 200 rpm. Lectins unattached to the bacteria were removed by spinning down the cell suspension (4000 rpm, 10 min) and washing the solution twice. The solution was resuspended to an OD_{600} of 0.1 and 10 μL of the labeled cell suspension was pipetted between a glass slide (75 × 75 mm) and a coverslip (20 × 20 mm). The fluorescent intensity of the labeled cells was determined using a fluorescent microscope (Nikon Eclipse *Ti-E*).

2.6. EDC−NHS Coupling. Lectins were coupled to the Si wafer surfaces using EDC−NHS chemistry (Scheme S1B) following a standardized coupling protocol described in the works of Kim et al.[46] and Patel et al.[47] Briefly, Si wafers were cleaned in Piranha solution (3:1 v/v H_2SO_4/30% H_2O_2) at 120 °C for 30 min (**Caution**! strongly corrosive), then incubated with a 3% (v/v) solution of APTES in anhydrous toluene for 24 h to make an APTES film on the surface. Toluene was used to sonicate the substrates for 20 min. The surfaces were then cured at 100 °C for 24 h, followed by sonication in ultrapure water for 20 min. Substrates were then incubated in DMF including 5 mg/mL of SA and 5% (v/v) trimethylamine for 4 h. The surfaces were immersed in a solution of EDC (50 mg/mL) and NHS (5 mg/mL) in 0.25 M of MES (pH 6.0) for 3 h to introduce NHS ester groups over the substrates. Functionalized surfaces were then immobilized with WGA (same as PVDMA surfaces) followed by incubation with different concentrations of *E. coli* cell suspensions.

2.7. Limit of Detection Determination. Limit of detection (LOD) is reported in terms of a solution concentration and was calculated according to the International Conference on Harmonisation (ICH) definition. This uses a combination of (1) microscopic evaluation of cells captured on a surface after incubation at a given solution concentration and (2) standard deviation and slope of the response ($3 \times \sigma/m$), where σ is the standard deviation from the replicates' analysis near the detection limit, and m is the slope of the calibration curve.[48−50]

2.8. Live/Dead Assay. A live/dead assay was used to measure bacteria viability after surface capture following the procedure described in the LIVE/DEAD BacLight Bacterial Viability Kit, L7012.[51] Briefly, 2 μL of SYTO 9 and 2 μL of propidium iodide fluorescent dyes were added to 1 mL of NaCl 0.85 wt % solution and thoroughly mixed. Flat and nanopillar surfaces were spin-coated (1500 rpm, 15 s) with a 0.75 wt % solution of $PGMA_{56}$-*b*-$PVDMA_{175}$ and then functionalized with WGA. *E. coli* solution (1 mL) (10^4 cfu/mL) was then incubated on the surfaces. After 1 h, bacteria on each surface were stained with 200 μL of SYTO 9/propidium iodide mixture for 15 min in a light-protected environment. SYTO 9 penetrates into the membrane of all cells, whereas propidium iodide only permeates dead cells and reduces SYTO 9 fluorescence when both dyes are present.[51,52] Samples were then washed with the buffer to remove unattached dye and imaged with a fluorescent microscope.

2.9. Instrumentation. *2.9.1. Fourier Transform Infrared Spectroscopy.* A PerkinElmer attenuated total reflection−Fourier transform infrared spectroscopy (ATR−FTIR) was used to generate IR spectra and measure the peak intensity of the azlactone carbonyl group at 1818 cm^{-1}. Before analyzing the samples, ethanol was used to clean the crystal and the background spectrum of the diamond crystal was obtained (64 scans). The spectra acquired were examined, background-subtracted, and baseline-corrected by using Perkin software.

2.9.2. Ellipsometry. A J.A. Woollam M-2000U variable angle spectroscopic ellipsometer was used to determine the polymer film thickness spin-coated over the Si wafers (wavelength range 245−999 nm). Optical properties were explained by a Cauchy model, considering: (1) polymer layer represented a uniform layer and (2) the refractive indices for PVDMA and PGMA at 632 nm were considered as 1.52 and 1.50, respectively.[41]

2.9.3. Brightfield and Fluorescence Microscopy. An upright microscope (BX51, Olympus) and a fluorescent microscope (Eclipse *Ti-E*, Nikon) were used to take brightfield and fluorescent images of surfaces containing fluorescent lectins or captured bacteria. Lectin levels were quantified using NIS-Element software and reported as average fluorescent intensity per area ± standard deviation.

2.9.4. Scanning Electron Microscopy. Characterization of surfaces was performed using scanning electron microscopy (SEM; FEI VERSA 3D DUAL BEAM) at 10 kV under 25 000 and 65 000 magnification. Bacteria were fixed for 15 min with 2.5% glutaraldehyde, and dehydrated in isopropanol solution (70 wt %) for 15 min. Prior to SEM analysis, the surfaces were coated with a thin gold film (3.2 nm) using an EMS 150R plus rotary pumped coater (Electron Microscopy Science).

2.10. Image Analysis. ImageJ software was used to count the number of attached bacteria on the surfaces. Five to six representative images of each substrate were taken at different locations and reported as average ± standard deviation.

DOI: 10.1021/acs.biomac.9b00609
Biomacromolecules XXXX, XXX, XXX−XXX

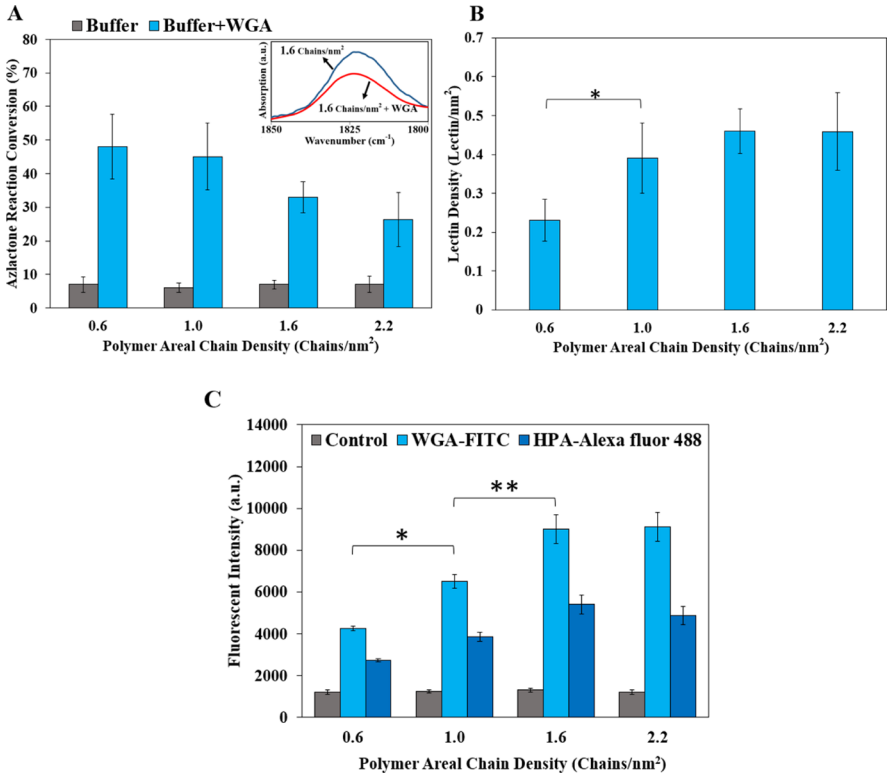

Figure 1. Surface characterization of lectin-functionalized $PGMA_{56}$-*b*-$PVDMA_{175}$ films using ellipsometry, ATR−FTIR, and fluorescent microscopy. (A) Azlactone reaction conversion after WGA coupling at each polymer surface density before and after WGA functionalization. (A inset) IR spectra of surfaces functionalized with 0.75 wt % polymer (blue line) and then coupled with WGA (red line). (B) WGA density measured for surfaces precoated with different polymer concentrations. (C) Fluorescent intensity of polymer-functionalized surfaces immobilized with 0.1 mg/mL of WGA−FITC or HPA−A488 in 1× PBS (control: 1× PBS without lectin incubated over substrates). ** = $P < 0.01$, * = $P < 0.05$, statistical differences apply to both WGA and HPA data sets. $n = 3$ independent substrates per condition. Values are the average ± standard deviation.

2.11. Statistical Analysis of Data. One-way ANOVA was used to compare group means and to test whether there was any statistical evidence that the associated population means were significantly different.[53] Post-hoc Tukey's tests were used to make pair-wise comparisons.[54] The statistical significance of the results was confirmed at 95% confidence level. Calculations were performed by MINITAB 17 software and all values reported as the mean with the standard deviation.

3. RESULTS AND DISCUSSION

3.1. Investigation of Lectin−Polymer Interactions on Flat Substrates. The goal of this study was to investigate the effect of PVDMA chain density on lectin coupling in an effort to identify the polymer chain densities that provide the highest levels of azlactone conversion and highest corresponding lectin density. Whereas higher PVDMA chain densities, and thus higher densities of azlactone groups, would be expected to increase lectin surface loading, other factors including steric hindrance of polymer brushes or changes in polymer morphology could render higher fractions of azlactone groups inaccessible for coupling. To investigate this, different concentrations of polymer (0.25−1 wt %) were first spin-coated over Si wafers followed by annealing and sonication.[55,56] Polymer film thickness and IR spectra of each sample were then measured (Figures S2 and S3) and subsequent calculation of areal chain densities was calculated using eq 1. Film thickness and areal chain density showed a linear increase with polymer solution concentration, consistent with Lokitz et al.[41] The overall range of thickness was found to be 30−110 nm, whereas the areal chain density was 0.5−2.2 chains/nm^2. Further, ATR−FTIR characterization of these substrates after WGA lectin coupling showed the expected decrease in the peak at 1818 cm^{-1} because of the ring opening, covalent reaction between azlactones and lectins,[29,57] and a corresponding appearance of an amide peak at ∼1600 cm^{-1} (Figure S3).

Azlactone conversion measured for each PVDMA chain density is shown in Figure 1A, as well as representative FTIR spectra of azlactone peak absorbance (inset). To account for the fact that azlactone hydrolysis from aqueous buffer could also cause a decrease in absorbance, control substrates that were incubated with coupling buffer only (1× PBS) were also measured, and showed 6−7% hydrolysis in every case, independent of PVDMA chain density. With lectin coupling, a significant portion of azlactone groups remained unreacted at each polymer density. Whereas this is partially due to the hydrophobic nature of the polymer that results in collapse of VDMA chains, a decrease in azlactone conversion with higher PVDMA chain densities is also noted. This trend suggests that as polymer chains become more compact, steric hindrance reduces the intermolecular interaction between lectin and polymer brushes.[58−60] A comparison of *P*-values from azlactone conversion data in Figure 1A reveals that the most significant impact of polymer chain density occurred between 1.0 and 1.6 chains/nm^2. Comparable trends have been noted with other PVDMA systems. For example, Aden et al. studied the surface properties and the reaction of PVDMA films with molecule amines (hexylamine, tetradecylamine, and octadecyl-

DOI: 10.1021/acs.biomac.9b00609
Biomacromolecules XXXX, XXX, XXX−XXX

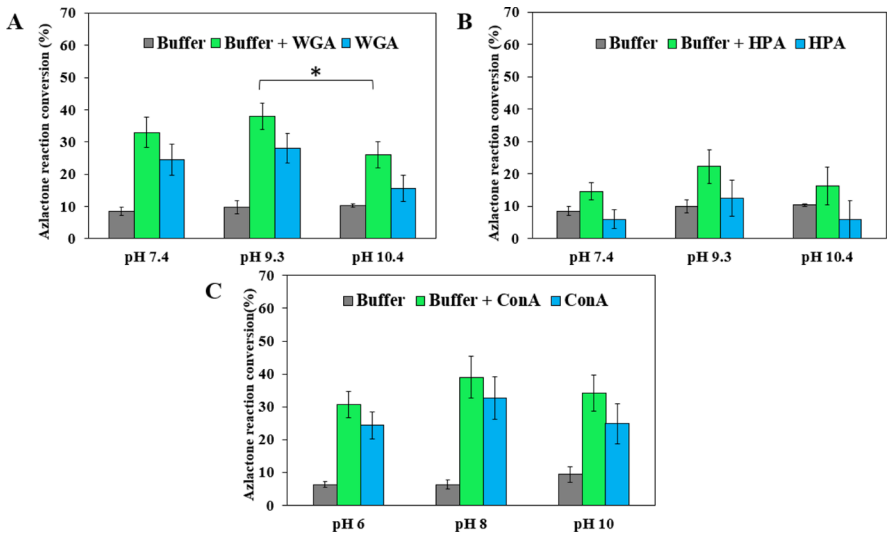

Figure 2. Results demonstrating the lectin addition and hydrolysis of azlactone groups at various pH. Variation of azlactone reaction conversion with different pH levels calculated by the percentage decrease in the height of the IR spectra peak at 1818 cm^{-1} because of (A) WGA immobilization, (B) HPA, and (C) ConA. Contribution of each lectin was measured by subtracting the summation (buffer + lectin) from hydrolysis data (buffer). * = $P < 0.05$, $n = 3$ independent substrates per condition. Values are the average ± standard deviation.

amine) and concluded that the degree of functionalization is lowered when the chain density of polymers increases.[61] In another work, neutron reflectometry analysis of PVDMA brushes coupled with amines indicated that the degree of functionalization of polymer decreases when the grafting density of brush chains increases.[42] We further estimated the resulting lectin density on these surfaces by assuming that conversion of one azlactone group was equivalent to attachment of one lectin, shown in Figure 1B. As evident, applying higher polymer concentrations results in more lectin density up to a polymer density of 1.6 chains/nm^2; beyond this point there was no change.

To verify the trends in Figure 1A,B, independent fluorescent measurements of lectin density were also performed using fluorescently labeled lectins (WGA−FITC and HPA−Alexa 488). Figure 1C shows the fluorescent intensity of polymer-functionalized substrates before and after treatment with solutions of WGA. The plot reveals increases in lectin density because of higher fluorescent intensity with increasing polymer concentration up to 1.6 chains/nm^2, followed by saturation at higher densities, consistent with the trend in Figure 1B, providing additional evidence of steric hindrance at higher polymer densities. To investigate if similar trends were noted with other lectins, analogous studies were performed with a significantly larger lectin (HPA ≈ 70 kDa compared to WGA ≈ 35 kDa), which showed a similar trend. It is worth mentioning that the intention of Figure 1C is not to compare the florescent intensity of WGA−FITC with HPA−Alexa fluor 488 at each polymer concentration, as each has been conjugated with a different type and number of fluorophores. These combined results led us to use surfaces with a chain density of 1.6 chains/nm^2 in order to provide maximum lectin loading for further use.

3.2. Investigation of a Lectin Panel for PVDMA Coupling and Microbe Capture. Despite the widespread potential to functionalize PVDMA-based polymers with biomolecules, coupling buffers that maximize PVDMA conversion with lectins have not been studied. Schmitt et al. reported that peptide coupling was significantly affected by change in pH, as an increase of pH from 7.4 to 9.5 enabled optimum coupling efficiency of cRGDfK peptides to PVDMA.[31] Here, the effect of coupling buffers on WGA, HPA, and ConA lectins was investigated using buffers with pH values commonly used in the literature.[40,62−65] The selection of these three lectins and the pH values tested were based on differences in molecular weight, isoelectric point, number of azlactone-reactive lysine residues, and sugar specificity (Table S1). Whereas higher pH buffers favor nucleophilic addition with primary amino nucleophiles, the rate of azlactone hydrolysis will also increase and consequently compromise the reactive groups available. Figure 2A−C demonstrates the effect of solution pH on hydrolysis and aminolysis of the azlactone ring. Here, azlactone reaction conversion was again measured using ATR−FTIR to identify the optimum pH, leading to the highest conversion for each lectin. Polymer-functionalized surfaces were also exposed to each buffer without lectin to quantify the effect from azlactone hydrolysis. The percentage decrease in the 1818 cm^{-1} peak can be attributed to the sum of the reactions of azlactone with amines and hydroxyl groups. The net contribution of amines then can be calculated by subtracting the summation from hydrolysis data. As can be seen for all three lectins, increasing pH to an intermediate level (pH 9.3 or 8.0) enhanced the lectin−azlactone reaction conversion marginally, reaching ∼30%. The optimal pH found at 9.3 is likely because this is slightly above the pK_a of lysine residues present on the protein (pK_a = 8.95),[66] resulting in deprotonated amino groups that most efficiently couple with the azlactones. The lower levels of HPA coupling compared to the other lectins may be due to the lower number of lysine residues present (Table S1).

To identify lectins that enable the highest bacteria capture levels, this panel of lectins was coupled to polymer surfaces at the pH showing highest levels of coupling, and capture levels for model *E. coli* mCherry cells at high concentrations (10^8 cfu/mL) were quantified. As lectins provide valuable interfaces for glycoprofiling cell-surfaces, proteins, and other glycoconjugates,[67] the secondary goal here was to verify that polymer-functionalized surfaces coupled with different lectins could

DOI: 10.1021/acs.biomac.9b00609
Biomacromolecules XXXX, XXX, XXX−XXX

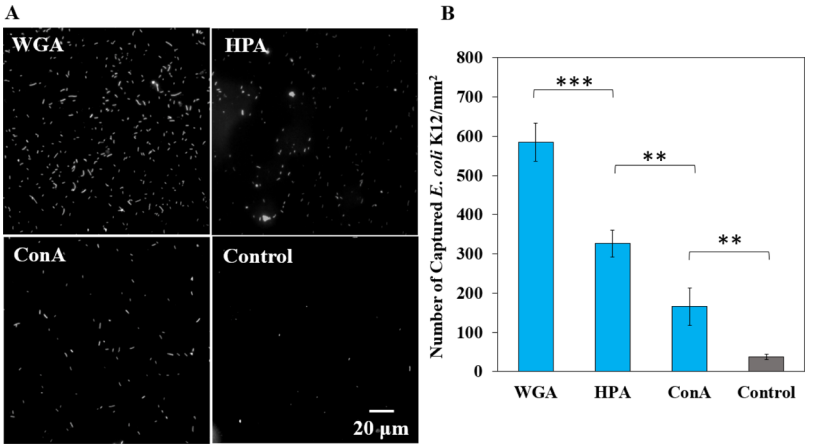

Figure 3. (A) Representative fluorescent images of *E. coli*-mCherry captured by the polymer surfaces immobilized with WGA, HPA, and ConA at high concentrations (10^8 cfu/mL). As the control, BSA solution (1 wt %) was incubated on the PVDMA substrates to account for nonspecific binding of cells to the surface under these conditions. (B) Calculated number of captured *E. coli* on the surface via using ImageJ. The values were given as the mean of five different surface locations from three independent surfaces. *** = $P < 0.001$, ** = $P < 0.01$. Values are the average ± standard deviation.

produce a differential binding response consistent with literature. The results in Figure 3 indicate that *E. coli* capturing capacity of WGA is higher than that of HPA and ConA, suggesting that WGA lectin had higher binding affinity for *E. coli* than HPA and ConA. The difference in capture ability might be due to the lectin size, sugar specificity, or the composition of the bacteria cell wall.[68] Similarly, Wang et al. described a surface plasmon resonance sensor coupled with WGA and ConA lectins for *E. coli* O157:H7 capture, also indicating higher capture of *E. coli* by WGA compared to ConA.[3] Hsu and Mahal reported a lectin microarray for fast analysis of the carbohydrates present on bacterial cell surfaces, and demonstrated that lectin surfaces produced differential binding levels, with WGA-functional surfaces capturing more *E. coli* compared to ConA.[69]

3.3. Characterization of PVDMA-Coated NPA Surfaces. In order to integrate physical nanostructures into our capture surfaces, we generated high-density NPAs on silicon surfaces using RIE etching, as described in Section 2.3. These structures were designed to serve as an underlying surface template for the PVDMA polymer films, providing the interface with pronounced nanoscale architecture. Etch times were varied to generate low-aspect ratio NPAs (LAR-NPAs) and high-aspect ratio NPAs (HAR-NPAs). Figure 4A,B show SEM images of substrates with LAR-NPA surfaces prior to the PVDMA coating step. These nanopillars appear to be 300 ± 59 nm in height with an average diameter of 73 ± 9 nm. After PVDMA spin-coating and annealing, the polymer appears visible on the nanopillars, as shown in Figure 4C. An increase in average pillar diameter to 120 ± 6 nm because of addition of the polymer coating was measured and pillar aggregation was also noted. The apparent thickness of the polymer films on nonaggregated pillars (~47 nm) was less than the polymer film thickness measured after spin-coating onto flat Si surfaces (80 nm, Figure S1), likely because the spin-coating process is nonconformal. HAR-NPA surfaces appeared to have similar pillar diameters as their LAR-NPA counterparts before coating, but the pillars were 2100 ± 126 nm in height, as shown in Figure 4D,E. After spin-coating over these surfaces, the polymer again appeared to cause nanopillar aggregation, as shown in Figure 4F. Because of excessive pillar aggregation

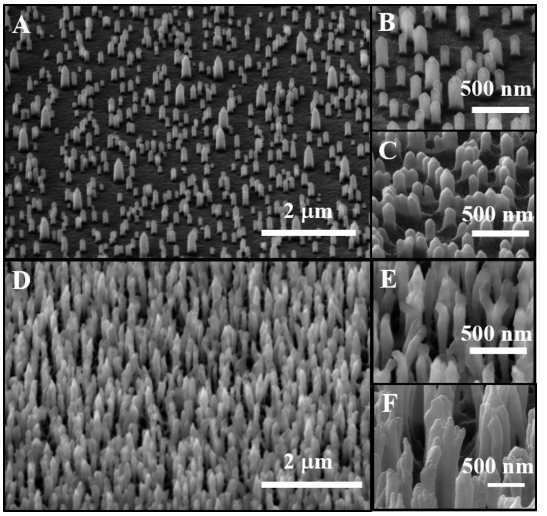

Figure 4. Scanning electron micrographs of NPAs before and after PVDMA spin-coating. (A,B) Uncoated LAR-NPA surfaces; (C) PVDMA-coated LAR-NPA surfaces; (D,E) uncoated HAR-NPA surfaces; (F) PVDMA-coated HAR-NPA surfaces. Spin-coating used a 0.75 wt % PVDMA solution followed by annealing at 110 °C.

here, we were unable to quantify the increase in individual pillar diameter because of the polymer. Instead, to further confirm the presence of the PVDMA polymer on the nanopillars, additional qualitative characterizations were made, including energy-dispersive X-ray spectroscopy to verify a change in surface composition and fluorescence measurements of the coated substrates (Figure S4), which detected an increase in fluorescence after the spin-coating and annealing steps because the polymer is weakly autofluorescent.

3.4. Sensitivity and Quantitative Detection of *E. coli*. Results obtained from Sections 3.1 to 3.3 were applied to generate both flat and NPA surfaces coated with lectin-functional PVDMA for assessment of capture sensitivity. All polymer films were functionalized under conditions showing highest levels of lectin coupling and bacteria capture at high concentrations (0.75 wt % PVDMA spin-coating, WGA lectin, pH 9.3 coupling buffer) and a set of capture experiments were performed to quantify the LOD.

DOI: 10.1021/acs.biomac.9b00609
Biomacromolecules XXXX, XXX, XXX−XXX

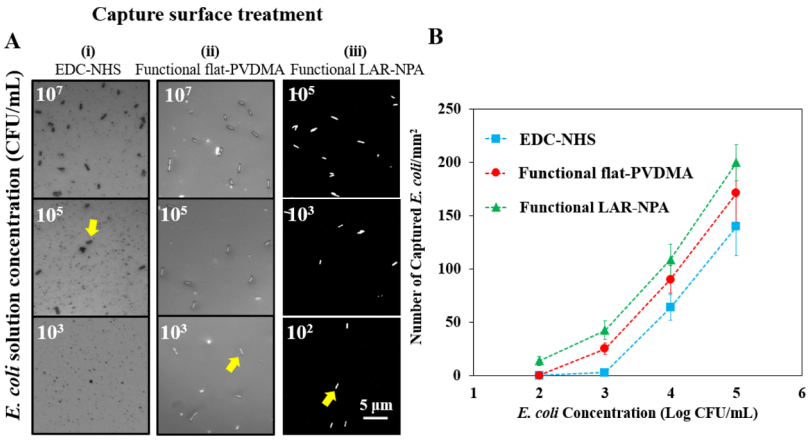

Figure 5. (A) Representative microscopic images of *E. coli* captured by the WGA immobilized on EDC−NHS surfaces, functional flat-PVDMA surfaces, and functional LAR-NPA surfaces after contact with bacteria at different concentrations. Yellow arrows indicate a representative bacteria cell on the surface. (B) Corresponding analysis of the number of captured *E. coli* for different bacteria solution concentrations. The values were given as the mean of five different locations from three independent surfaces. Values are the average ± standard deviation.

To first benchmark the gains in sensitivity from the flat polymer surfaces against standardized capture substrates, a side-by-side comparison of capture levels was performed using lectin substrates functionalized with an EDC−NHS coupling chemistry protocol.[46] Different concentrations of bacterial culture (ranging from 10^2 to 10^5 cfu/mL) were contacted with WGA functionalized to either flat PVDMA or EDC−NHS surfaces and incubated for 1 h (Figure 5A(i),(ii)). For a wider observation of these surfaces, see Figure S5. For flat, WGA-functionalized PVDMA surfaces (herein referred to as functional flat-PVDMA), the number of cells captured was significantly higher at concentrations between 10^3 and 10^4 cfu/mL ($P < 0.01$), as shown in Figure 5B. An estimated detection limit of 1.7×10^3 cfu/mL was calculated and a linear correlation between the number of captured bacteria and the logarithm of *E. coli* concentration was also observed. The result at 10^3 cfu/mL (Figure 5A(ii)) was presented to demonstrate bacteria capture near the LOD. For control EDC−NHS substrates, no bacteria were observed at a concentration of 10^3 cfu/mL, and the LOD was estimated as 1.6×10^4 cfu/mL. Compared with the EDC−NHS cross-linking protocol, the functional flat-PVDMA surface exhibited a lower detection limit by roughly 1 order of magnitude. This improvement in sensitivity is attributed to the increased lectin density and uniformity over the PVDMA polymer. We quantified that a 41.9% increase in lectin density was present relative to the control, based on fluorescence measurement (Figure S6). Further comparison of capture levels at diluted bacteria concentrations (10^4 cfu/mL) also shows that capture efficiency, defined as the number of cells captured on the surface compared to the number of cells initially in solution, improved from 51.8 to 72.9%.

This comparison quantifies the gains in sensitivity that can be achieved using the polymer compared to conventional interface chemistry. Additional advantages of using the polymer relative to the standard substrates include (1) high hydrolytic stability of PVDMA compared to NHS esters, which are susceptible to hydrolysis,[25] making it a more robust platform for biofunctionalization; (2) a facile, one-step protein bioconjugation using a rapid "click" reaction with no byproducts; and (3) facile control of reactive site densities through modulating the polymer solution deposition procedure (Figure S2). This last benefit is particularly useful, as it enables one to modulate the range and strength of the cell-binding interaction.

To access the impact of incorporating nanostructure into the lectin-functionalized polymer films, the sensitivity was accessed in an analogous fashion for NPA surfaces after PVDMA-coating and WGA functionalization; these surfaces are herein referred to as "functional NPAs". Figure 5 demonstrates additional gains in capture efficiency and sensitivity using the functional LAR-NPA surfaces, as cell capture levels were significantly increased at all solution concentrations between 10^2 and 10^4 cfu/mL ($P < 0.01$). With the addition of the LAR-NPAs, the LOD using the PVDMA coatings improved from 1.7×10^3 to 2.1×10^2 cfu/mL. Binary fluorescent images instead of brightfield images are provided for the functional LAR-NPA surfaces for image clarity (Figure 5A(iii)). To check for nonspecific capture of bacteria because of the presence of the nanostructures, a negative control was performed by instead passivating LAR-NPA surfaces with BSA. Here, capture of *E. coli* was minimal (12 ± 3 cells/mm^2) at solution concentrations of 10^4 cfu/mL. Capture on functional HAR-LAR surfaces was not quantified, as distinctive changes in cell morphology were noted; this will be discussed in Section 3.5.

The positive effects from the nanostructure are consistent with multiple findings from the literature. For example, Jalali et al. presented a microfluidic device containing three-dimensional, shrub-like nano−micro islands (NMI) for capture and detection of *E. coli* and *Staphylococcus aureus*. The fluorescent intensity of both captured on 3D NMI structures was improved compared to flat platforms.[70] With respect to eukaryotic cell capture, Wang et al. reported Si NPAs immobilized with epithelial-cell adhesion-molecule antibodies to isolate circulating tumor cells and found that the functionalized NPAs increased cell adhesion 10-fold compared to smooth Si substrates.[71] Chen et al. measured a similar increase in CTC capture by increasing the roughness of the capture surface from 1 to 150 nm.[72]

The gains in sensitivity quantified for lectin-based capture from (i) use of the PVDMA polymer and (ii) addition of nanostructure give these interfaces relevance to a variety of different diagnostic applications where lectin-based bacteria capture is traditionally limited. For example, contaminated water samples containing fecal coliforms such as *Enterococci* and *Escherichia* bacteria generally range in concentrations from

DOI: 10.1021/acs.biomac.9b00609
Biomacromolecules XXXX, XXX, XXX−XXX

10^3 to 10^5 cfu/mL.[73,74] With respect to clinical applications, urinary tract infections (UTIs) often require detection on the order of 10^3 cfu/mL, depending on the type of bacteria present.[75] Both flat and NPA surfaces are applicable for UTI diagnosis. Finally, literature reports the initial symptoms of sepsis in an adult when bacteria are present in blood at 1−100 cfu/mL.[76,77] Lectins have been shown to be particularly useful for isolation of bacteria from blood; for example, engineered mannose binding lectin was recently applied to remove Gram-negative and Gram-positive pathogens from blood at high specificity in a blood cleansing device.[15] Our highest sensitivity surfaces, achieved with functional LAR-NPAs surfaces, achieves an LOD on the order of 10^2 cfu/mL, approaching the upper-end of the sensitivity requirement for applications to blood infections. Whereas further development is required for bacteria isolation directly from clinical or environmental samples, we have observed similar capture levels between the buffer and the LB media (Figure S7), suggesting that these surfaces are useful for capture from more complex media.

3.5. Bacteria Viability after Capture on Functional NPA Surfaces. Whereas functional NPAs improved cell capture, nanopillars may also have bactericidal properties as they can cause mechanical cell deformation and lysis by puncturing and rupturing the cell membrane on contact.[78] To characterize the effect of the nanopillar structure on cell viability, both SEM images and live/dead assays were used. Figure 6A shows the SEM images of *E. coli* after capture on

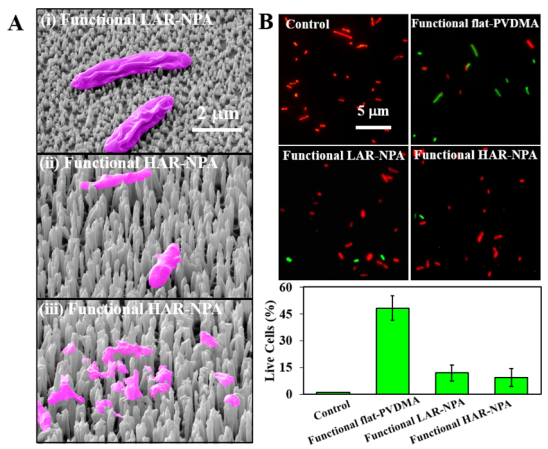

Figure 6. (A) Scanning electron micrographs and microscopic images of *E. coli* after capture onto functional NPA surfaces. Bacteria or cellular debris were colored pink to distinguish them from the pillars. (B) Representative fluorescent images and % of live cells after capture to each surface. Control: attached bacteria were exposed to a 2.5% glutaraldehyde solution and 70% isopropanol solution to verify that dead cells could be detected with the live/dead assay. Live/dead assay images were adjusted with ImageJ to maximize color contrast.

functional LAR-NPA and functional HAR-NPA surfaces. Whereas the cell structure was maintained on LAR-NPA surfaces (Figure 6A(i)), significant deformation in cell morphology becomes apparent on HAR-NPA surfaces. Here, intact bacteria appear more stretched and deformed across the pillars (Figure 6A(ii)) and cellular debris also becomes visible across the surface (Figure 6A(iii)), indicating that cell lysis is occurring. Live-dead assays indicate that while 48 ± 6.8% of the attached *E. coli* cells remained alive after contact on the flat PVDMA surfaces, viability decreased upon contact with the NPAs; 12 ± 4.5% of cells were live on LAR-NPAs and 9 ± 4% of intact cells were alive on HAR-NPAs (Figure 6B). Taken together, the combined results in Figures 5 and 6 emphasize the potential trade-offs offered by each capture surface. For applications where only capture and detection sensitivity are important, LAR-NPA surfaces are most beneficial. However, for applications requiring retrieval of live cells for culture-based follow-up analysis (e.g., enrichment for genotyping, testing for antibiotic resistance, etc.), nonstructured, flat PVDMA surfaces may be more beneficial.

3.6. Importance of Bacteria UPP Expression Versus Lectin Density on Capture. Whereas lectin density is key for improving bacteria capture, the structure and composition of the bacteria's extracellular surface can also play a significant role.[36] Here, we systematically modulated production of an exopolysaccharide adhesin, a critical bacterial cell surface feature, to understand its effect on lectin-based surface capture. This was achieved using *A. tumefaciens* JX110 pJW110, a mutant strain that produces modulated levels of UPP adhesin in response to varied degree of pleD gene expression. The UPP adhesin is localized to one pole of *A. tumefaciens* cells and plays a key role in initiating stable surface attachment.[36,79] Extracellular UPP levels can be controlled by varying IPTG inducer concentration in culture media. Without IPTG induction, very low levels of UPP are inherently present and this strain also lacks other major exopolysaccharides produced by *A. tumefaciens*. Upon induction, UPP is produced and binds WGA lectin because it is partly composed of *N*-acetyl glucosamine (GlcNAc) components. Consequently, this system allows us to experimentally manipulate the degree to which bacterial cells present extracellular surface features required for capture by lectin-functional interfaces. Further, this experimental system allows us to manipulate these features over a broad and quantitative range, including levels exceeding that of unmanipulated, planktonic *A. tumefaciens* cells.[37]

It was first verified that UPP expression could be modulated by culturing JX110 pJW110 in culture media supplemented with either 0, 50, 100, 200, or 400 μM IPTG. Similar experimental conditions reported in Xu et al. were sufficient to produce substantial overexpression of the UPP adhesin relative to uninduced controls.[37] Extracellular glycan levels were then characterized with a solution-phase lectin binding assay using WGA−FITC, binding to GlcNAc components present on the extracellular surface.[29] As shown in Figure 7A, increasing the IPTG concentration resulted in proportionally higher UPP production consistent with the results of Xu et al.[37] Post hoc Tukey's test was applied to identify three groups with significantly different fluorescence levels (denoted by groups a, b, and c in Figure 7A). On the basis of this, we used IPTG concentrations of 0, 200, and 400 μM for subsequent experiments in which cells produced varying levels of UPP ($P < 0.05$). Across this range of IPTG concentrations, a wide range of UPP levels was achieved for further study; increasing IPTG from 0 to 200 μM raised the cell fluorescent intensity by 96%, whereas an additional increase to 400 μM increased cell fluorescence by another 35%. To measure the impact that UPP production levels had on capture, WGA surface density was held constant (0.46 lectins/nm^2) and capture was measured by incubating the surfaces with JX110 pJW110 populations cultured at each of the three different IPTG concentrations identified from Figure 7A. Each population was incubated over the lectin-functional surface at the same concentration (OD_{600} = 0.1) and experimental conditions. As shown in Figure 7B, a slight increase in bacteria capture was measured as UPP

DOI: 10.1021/acs.biomac.9b00609
Biomacromolecules XXXX, XXX, XXX−XXX

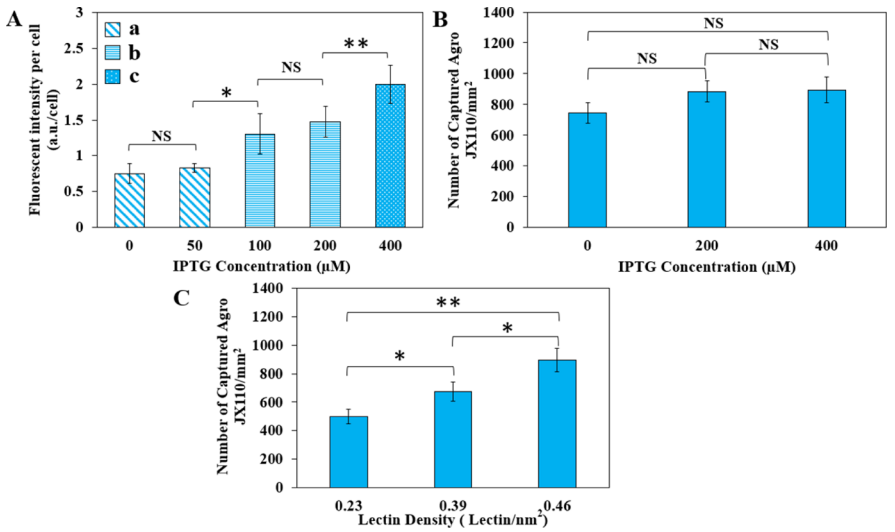

Figure 7. (A) Variation of fluorescent intensity of *A. tumefaciens* JX110 cells after culturing at different IPTG concentrations and labeling with FITC-conjugated WGA lectins. One-way ANOVA and Tukey's test were applied to measure overall and pairwise p-values, respectively. Tukey test categorized IPTG concentrations into three different groups (a, b, and c). (B) Number of captured *A. tumefaciens* JX110 cells on the surface at different IPTG concentrations. All solutions of JX110 cells were incubated on the surface at OD 0.1 and lectin density was held constant at 0.46 WGA/nm^2. (C) Number of captured *A. tumefaciens* JX110 on the surface at different lectin densities. All solutions were again incubated over the surface at OD 0.1 and the IPTG concentration was kept constant at 200 μM. The values were given as the mean of five different locations from three independent surfaces. ** = $P < 0.01$, * = $P < 0.05$, NS = not significant. Values are the average ± standard deviation.

expression increased. However, the difference was not statistically significant ($P > 0.05$). To compare these changes to changes caused by varying the WGA surface density, populations of cells showing intermediate levels of UPP expression (IPTG = 200 μM) were cultured; then their capture was measured across surfaces with varied WGA densities (Figure 7C). JX110 pJW110 populations were incubated over the surface at the same concentration as in the previous experiment (OD_{600} = 0.1). Here, the number of captured bacteria showed a strong dependence on WGA density, as increasing WGA densities from 0.23 to 0.39 or to 0.46 WGA/nm^2 generated significant increases in capture ($P < 0.05$). Results from Figure 7A,B demonstrate that bacteria capture increases as both the levels of extracellular adhesin increase and as lectin surface densities increase, which is consistent with other reports,[9,80−82] and with the theory that multivalent lectin−oligosaccharide interactions increase binding strength.[18,83] Comparing the two different factors, it appears that lectin surface densities had a greater impact on capture efficiency as a twofold increase in lectin density generated a statistically significant increase in capture level, whereas a threefold increase in extracellular glycosylation levels did not. This finding is highly favorable, because in real capture applications the lectin surface density on the synthetic interface can be easily manipulated using the parameters discussed previously (see Figures 1−4), whereas the extracellular glycan levels of the targeted bacteria cannot be controlled. This highlights the importance of the synthetic interface for driving capture and for loading high levels of lectin to the surface in order to efficiently capture bacteria as they encounter the surface.

4. CONCLUSIONS

Lectin proteins bind extracellular glycan structures with high specificity and can be functionalized to synthetic interfaces for nondestructive cell capture and glycomic profiling. In the present research we performed a systematic study of parameters that influence lectin coupling to the azlactone-functional block copolymer, $PGMA_{56}$-*b*-$PVDMA_{175}$, and used these findings to construct capture surfaces with maximized lectin density and pronounced nanoscale surface structures for highest capture efficiency and detection sensitivity at 10^2 cfu/mL. It was shown that applying higher polymer concentrations led to higher lectin surface density up to a polymer density of 1.6 chains/nm;^{2} further increases did not impact lectin density, likely because of steric hindrance. Functional NPA surfaces were able to provide more interaction area with cells to enhance cell capture. Gains in *E. coli* capture on flat and nanopillar surfaces were quantified, and compared to standard carbodiimide (EDC−NHS) coupling (LOD: 1.6×10^4 cfu/mL); 1 order of magnitude improvement in detection sensitivity was achieved by introducing the functional polymer to flat surfaces (LOD: 1.7×10^3 cfu/mL), whereas 2 orders of magnitude improvement in detection sensitivity was measured for the nanopillar surface (LOD: 2.1×10^2 cfu/mL). The range of detection sensitivities achieved for our flat and NPA surfaces offer potential use in a variety of applications including diagnosis of UTI, blood infections, and detection of bacterial pathogens in water-applications where lectin-based capture has traditionally been limited. Finally, our experiments indicate that lectin surface density, modulated by the underlying polymer chain density, allows for one to efficiently tune the strength of the binding interaction, and that this parameter had a greater impact than extracellular glycosylation levels on bacterial cell capture. Taken together, this work emphasizes the critical role of the synthetic interface design for efficient isolation of bacteria from solutions.

■ ASSOCIATED CONTENT

Supporting Information

The Supporting Information is available free of charge on the ACS Publications website at DOI: 10.1021/acs.biomac.9b00609.

DOI: 10.1021/acs.biomac.9b00609
Biomacromolecules XXXX, XXX, XXX−XXX

$PGMA_{56}$-*b*-$PVDMA_{175}$ and EDC/NHS surface functionalization scheme; growth curve of the *A. tumefaciens* JX110 culture solution; ellipsometry analysis of Si surfaces spin-coated with different polymer concentrations; ATR−FTIR analysis of Si surfaces spin-coated with different polymer concentrations; SEM−EDX and autofluorescence analysis of bare Si and PVDMA-coated surfaces; microscopic images of *E. coli* captured on Si surfaces functionalized with $PGMA_{56}$-*b*-$PVDMA_{175}$ and EDC/NHS treatment method at different bacteria concentrations; representative fluorescent images of lectin surfaces functionalized using EDC/NHS and VDMA coupling; comparison of bacteria capture from 1× PBS and LB media; and properties of the lectin panel used (PDF)

AUTHOR INFORMATION

Corresponding Author

*E-mail: rrhansen@ksu.edu. Phone: (785) 532-0625.

ORCID

Mohammadali Masigol: 0000-0002-3367-7646

Bradley S. Lokitz: 0000-0002-1229-6078

Ryan. R. Hansen: 0000-0002-6471-047X

Author Contributions

The paper was written through contributions of all the authors. All the authors have given approval to the final version of the paper.

Notes

The authors declare no competing financial interest.

This paper has been authored by UT-Battelle, LLC under contract no. DE-AC05-00OR22725 with the U.S. Department of Energy. The United States Government retains and the publisher, by accepting the article for publication, acknowledges that the United States Government retains a nonexclusive, paid-up, irrevocable, worldwide license to publish or reproduce the published form of this paper, or allow others to do so, for United States Government purposes. The Department of Energy will provide public access to these results of federally sponsored research in accordance with the DOE Public Access Plan (http://energy.gov/downloads/doe-public-access-plan).

ACKNOWLEDGMENTS

This research was supported by Kansas State University. A portion of this research was conducted at the Center for Nanophase Materials Sciences, which is sponsored at Oak Ridge National Laboratory by the Scientific User Facilities Division, Office of Basic Energy Sciences and U.S. Department of Energy. We thank Dr. Clay Fuqua (Department of Biology, Indiana University, Bloomington) for providing bacteria strains. We also would like to express our appreciation to Dr. André J. van der Vlies for his valuable and constructive comments during the planning and development of the presented work and Dr. Prem Thapa (Microscopy and Analytical Imaging, Laboratory at University of Kansas) for assistance with SEM imaging.

REFERENCES

(1) Shen, Z.; Huang, M.; Xiao, C.; Zhang, Y.; Zeng, X.; Wang, P. G. Nonlabeled Quartz Crystal Microbalance Biosensor for Bacterial Detection using Carbohydrate and Lectin Recognitions. *Anal. Chem.* **2007**, *79*, 2312−2319.

(2) Dechtrirat, D.; Gajovic-Eichelmann, N.; Wojcik, F.; Hartmann, L.; Bier, F. F.; Scheller, F. W. Electrochemical Displacement Sensor Based on Ferrocene Boronic Acid Tracer and Immobilized Glycan for Saccharide Binding Proteins and E. Coli. *Biosens. Bioelectron.* **2014**, *58*, 1−8.

(3) Wang, Y.; Ye, Z.; Si, C.; Ying, Y. Monitoring of Escherichia coli O157:H7 in food samples using lectin based surface plasmon resonance biosensor. *Food Chem.* **2013**, *136*, 1303−1308.

(4) Zheng, L.; Wan, Y.; Qi, P.; Sun, Y.; Zhang, D.; Yu, L. Lectin Functionalized ZnO Nanoarrays as a 3D Nano-Biointerface for Bacterial Detection. *Talanta* **2017**, *167*, 600−606.

(5) Serra, B.; Gamella, M.; Reviejo, A. J.; Pingarrón, J. M. Lectin-Modified Piezoelectric Biosensors for Bacteria Recognition and Quantification. *Anal. Bioanal. Chem.* **2008**, *391*, 1853−1860.

(6) Poonlapdecha, W.; Seetang-Nun, Y.; Wonglumsom, W.; Tuitemwong, K.; Erickson, L. E.; Hansen, R. R.; Tuitemwong, P. Antibody-Conjugated Ferromagnetic Nanoparticles with Lateral Flow Test Strip Assay for Rapid Detection of Campylobacter Jejuni in Poultry Samples. *Int. J. Food Microbiol.* **2018**, *286*, 6−14.

(7) Thepwiwatjit, N.; Thattiyaphong, A.; Limsuwan, P.; Tuitemwong, K.; Tuitemwong, P. Rubpy Dye-Doped Silica Nanoparticles as Signal Reporter in a Dot Fluorescence Immunoassay Strip. *J. Nanomater.* **2014**, *2014*, 851905.

(8) Tansub, W.; Tuitemwong, K.; Limsuwan, P.; Theparoonrat, S.; Tuitemwong, P. Synthesis of Antibodies-Conjugated Fluorescent Dye-Doped Silica Nanoparticles for a Rapid Single Step Detection of Campylobacter Jejuni in Live Poultry. *J. Nanomater.* **2012**, *2012*, 865186.

(9) Gamella, M.; Campuzano, S.; Parrado, C.; Reviejo, A. J.; Pingarrón, J. M. Microorganisms Recognition and Quantification by Lectin Adsorptive Affinity Impedance. *Talanta* **2009**, *78*, 1303−1309.

(10) Huang, C.-C.; Chen, C.-T.; Shiang, Y.-C.; Lin, Z.-H.; Chang, H.-T. Synthesis of Fluorescent Carbohydrate-Protected Au Nanodots for Detection of Concanavalin A andEscherichia coli. *Anal. Chem.* **2009**, *81*, 875−882.

(11) Sharon, N. Lectins: Carbohydrate-Specific Reagents and Biological Recognition Molecules. *J. Biol. Chem.* **2007**, *282*, 2753−2764.

(12) Vickers, D. A.; Kulik, M.; Hincapie, M.; Hancock, W. S.; Dalton, S.; Murthy, S. K. Lectin-Functionalized Microchannels for Characterizing Pluripotent Cells and Early Differentiation. *Biomicrofluidics* **2012**, *6*, 024122.

(13) Vickers, D. A. L.; Hincapie, M.; Hancock, W. S.; Murthy, S. K. Lectin-Mediated Microfluidic Capture and Release of Leukemic Lymphocytes from Whole Blood. *Biomed. Microdevices* **2011**, *13*, 565−571.

(14) Campuzano, S.; Orozco, J.; Kagan, D.; Guix, M.; Gao, W.; Sattayasamitsathit, S.; Claussen, J. C.; Merkoçi, A.; Wang, J. Bacterial Isolation by Lectin-Modified Microengines. *Nano Lett.* **2011**, *12*, 396−401.

(15) Kang, J. H.; Super, M.; Yung, C. W.; Cooper, R. M.; Domansky, K.; Graveline, A. R.; Mammoto, T.; Berthet, J. B.; Tobin, H.; Cartwright, M. J.; Watters, A. L.; Rottman, M.; Waterhouse, A.; Mammoto, A.; Gamini, N.; Rodas, M. J.; Kole, A.; Jiang, A.; Valentin, T. M.; Diaz, A.; Takahashi, K.; Ingber, D. E. An Extracorporeal Blood-Cleansing Device for Sepsis Therapy. *Nat. Med.* **2014**, *20*, 1211.

(16) Bewley, C. A.; Shahzad-ul-Hussan, S. Characterizing Carbohydrate-Protein Interactions by Nuclear Magnetic Resonance Spectroscopy. *Biopolymers* **2013**, *99*, 796−806.

(17) Liang, P.-H.; Wang, S.-K.; Wong, C.-H. Quantitative Analysis of Carbohydrate−Protein Interactions Using Glycan Microarrays: Determination of Surface and Solution Dissociation Constants. *J. Am. Chem. Soc.* **2007**, *129*, 11177−11184.

(18) Kluková, L.; Bertok, T.; Kasák, P.; Tkac, J. Nanoscale-Controlled Architecture for the Development of Ultrasensitive Lectin Biosensors Applicable in Glycomics. *Anal. Methods* **2014**, *6*, 4922−4931.

DOI: 10.1021/acs.biomac.9b00609
Biomacromolecules XXXX, XXX, XXX−XXX

(19) Templier, V.; Roux, A.; Roupioz, Y.; Livache, T. Ligands for Label-Free Detection of Whole Bacteria on Biosensors: A Review. *TrAC, Trends Anal. Chem.* **2016**, *79*, 71−79.
(20) Belicky, t.; Katrlik, J.; Tkac, J. Glycan and Lectin Biosensors. *Essays Biochem.* **2016**, *60*, 37−47.
(21) Zayas-Gonzalez, Y. M.; Lynn, D. M. Degradable Amine-Reactive Coatings Fabricated by the Covalent Layer-by-Layer Assembly of Poly(2-vinyl-4,4-dimethylazlactone) with Degradable Polyamine Building Blocks. *Biomacromolecules* **2016**, *17*, 3067−3075.
(22) Buck, M. E.; Lynn, D. M. Layer-by-Layer Fabrication of Covalently Crosslinked and Reactive Polymer Multilayers using Azlactone-Functionalized Copolymers: A Platform for the Design of Functional Biointerfaces. *Adv. Eng. Mater.* **2011**, *13*, B343−B352.
(23) Zayas-Gonzalez, Y. M.; Ortiz, B. J.; Lynn, D. M. Layer-by-Layer Assembly of Amine-Reactive Multilayers using an Azlactone-Functionalized Polymer and Small-Molecule Diamine Linkers. *Biomacromolecules* **2017**, *18*, 1499−1508.
(24) Schmitt, S. K.; Trebatoski, D. J.; Krutty, J. D.; Xie, A. W.; Rollins, B.; Murphy, W. L.; Gopalan, P. Peptide Conjugation to a Polymer Coating Via Native Chemical Ligation of Azlactones for Cell Culture. *Biomacromolecules* **2016**, *17*, 1040−1047.
(25) Cullen, S. P.; Mandel, I. C.; Gopalan, P. Surface-Anchored Poly(2-vinyl-4,4-dimethyl azlactone) Brushes as Templates for Enzyme Immobilization. *Langmuir* **2008**, *24*, 13701−13709.
(26) Kratochvil, M. J.; Carter, M. C. D.; Lynn, D. M. Amine-Reactive Azlactone-Containing Nanofibers for the Immobilization and Patterning of New Functionality on Nanofiber-Based Scaffolds. *ACS Appl. Mater. Interfaces* **2017**, *9*, 10243−10253.
(27) Broderick, A. H.; Carter, M. C. D.; Lockett, M. R.; Smith, L. M.; Lynn, D. M. Fabrication of Oligonucleotide and Protein Arrays on Rigid and Flexible Substrates Coated with Reactive Polymer Multilayers. *ACS Appl. Mater. Interfaces* **2012**, *5*, 351−359.
(28) Neri, G.; Scala, A.; Barreca, F.; Fazio, E.; Mineo, P. G.; Mazzaglia, A.; Grassi, G.; Piperno, A. Engineering of Carbon Based Nanomaterials by Ring-Opening Reactions of a Reactive Azlactone Graphene Platform. *Chem. Commun.* **2015**, *51*, 4846−4849.
(29) Hansen, R. R.; Hinestrosa, J. P.; Shubert, K. R.; Morrell-Falvey, J. L.; Pelletier, D. A.; Messman, J. M.; Kilbey, S. M.; Lokitz, B. S.; Retterer, S. T. Lectin-Functionalized Poly(glycidyl methacrylate)-block-poly(vinyldimethyl azlactone) Surface Scaffolds for High Avidity Microbial Capture. *Biomacromolecules* **2013**, *14*, 3742−3748.
(30) Hansen, R.; Shubert, K.; Morrell-Falvey, J.; Lokitz, B.; Doktycz, M.; Retterer, S. Microstructured Block Copolymer Surfaces for Control of Microbe Adhesion and Aggregation. *Biosensors* **2014**, *4*, 63−75.
(31) Schmitt, S. K.; Xie, A. W.; Ghassemi, R. M.; Trebatoski, D. J.; Murphy, W. L.; Gopalan, P. Polyethylene Glycol Coatings on Plastic Substrates for Chemically Defined Stem Cell Culture. *Adv. Healthcare Mater.* **2015**, *4*, 1555−1564.
(32) Valle, J.; Burgui, S.; Langheinrich, D.; Gil, C.; Solano, C.; Toledo-Arana, A.; Helbig, R.; Lasagni, A.; Lasa, I. Evaluation of Surface Microtopography Engineered by Direct Laser Interference for Bacterial Anti-Biofouling. *Macromol. Biosci.* **2015**, *15*, 1060−1069.
(33) Friedlander, R. S.; Vlamakis, H.; Kim, P.; Khan, M.; Kolter, R.; Aizenberg, J. Bacterial Flagella Explore Microscale Hummocks and Hollows to Increase Adhesion. *Proc. Natl. Acad. Sci. U.S.A.* **2013**, *110*, 5624−5629.
(34) Agapov, R. L.; Boreyko, J. B.; Briggs, D. P.; Srijanto, B. R.; Retterer, S. T.; Collier, C. P.; Lavrik, N. V. Asymmetric Wettability of Nanostructures Directs Leidenfrost Droplets. *ACS Nano* **2013**, *8*, 860−867.
(35) Donlan, R. M. Biofilms: Microbial Life on Surfaces. *Emerg. Infect. Dis.* **2002**, *8*, 881−890.
(36) Tomlinson, A. D.; Fuqua, C. Mechanisms and Regulation of Polar Surface Attachment in Agrobacterium Tumefaciens. *Curr. Opin. Microbiol.* **2009**, *12*, 708−714.
(37) Xu, J.; Kim, J.; Koestler, B. J.; Choi, J.-H.; Waters, C. M.; Fuqua, C. Genetic analysis ofAgrobacterium tumefaciensunipolar polysaccharide production reveals complex integrated control of the motile-to-sessile switch. *Mol. Microbiol.* **2013**, *89*, 929−948.
(38) Xu, J.; Kim, J.; Danhorn, T.; Merritt, P. M.; Fuqua, C. Phosphorus Limitation Increases Attachment in Agrobacterium Tumefaciens and Reveals a Conditional Functional Redundancy in Adhesin Biosynthesis. *Res. Microbiol.* **2012**, *163*, 674−684.
(39) Gueffroy, D. E. *A Guide for the Preparation and Use of Buffers in Biological Systems*; Calbiochem-Behring Corporation, 1975.
(40) Zhuang, M.-Y.; Wang, C.; Xu, M. Q.; Ling, X. M.; Shen, J. J.; Zhang, Y. W. Using concanavalinA as a spacer for immobilization of E. coli onto magnetic nanoparticles. *Int. J. Biol. Macromol.* **2017**, *104*, 63−69.
(41) Lokitz, B. S.; Wei, J.; Hinestrosa, J. P.; Ivanov, I.; Browning, J. F.; Ankner, J. F.; Kilbey, S. M.; Messman, J. M. Manipulating Interfaces through Surface Confinement of Poly(glycidyl methacrylate)-block-poly(vinyldimethylazlactone), a Dually Reactive Block Copolymer. *Macromolecules* **2012**, *45*, 6438−6449.
(42) Aden, B.; Kite, C. M.; Hopkins, B. W.; Zetterberg, A.; Lokitz, B. S.; Ankner, J. F.; Kilbey, S. M. Assessing Chemical Transformation of Reactive, Interfacial Thin Films Made of End-Tethered Poly(2-vinyl-4,4-dimethyl azlactone) (PVDMA) Chains. *Macromolecules* **2017**, *50*, 618−630.
(43) Steglich, M.; Käsebier, T.; Zilk, M.; Pertsch, T.; Kley, E.-B.; Tünnermann, A. The Structural and Optical Properties of Black Silicon by Inductively Coupled Plasma Reactive Ion Etching. *J. Appl. Phys.* **2014**, *116*, 173503.
(44) Tempe, J.; Petit, A.; Holsters, M.; Montagu, M. v.; Schell, J. Thermosensitive Step Associated with Transfer of the Ti Plasmid during Conjugation: Possible Relation to Transformation in Crown Gall. *Proc. Natl. Acad. Sci. U.S.A.* **1977**, *74*, 2848−2849.
(45) Morton, E. R.; Platt, T. G.; Fuqua, C.; Bever, J. D. Non-Additive Costs and Interactions Alter the Competitive Dynamics of Co-Occurring Ecologically Distinct Plasmids. *Proc. Biol. Sci.* **2014**, *281*, 20132173.
(46) Kim, J. Chemical Modifications of Amino-Terminated Organic Films on Silicon Substrates and Controlled Protein Immobilization by FT-IR and Ellipsometry. *Spectroscopy-Eugene* **2012**, *25*, 26.
(47) Patel, N.; Davies, M. C.; Hartshorne, M.; Heaton, R. J.; Roberts, C. J.; Tendler, S. J. B.; Williams, P. M. Immobilization of Protein Molecules Onto Homogeneous and Mixed Carboxylate-Terminated Self-Assembled Monolayers. *Langmuir* **1997**, *13*, 6485−6490.
(48) Rengaraj, S.; Cruz-Izquierdo, Á.; Scott, J. L.; Di Lorenzo, M. Impedimetric Paper-Based Biosensor for the Detection of Bacterial Contamination in Water. *Sens. Actuators, B* **2018**, *265*, 50−58.
(49) Shrivastava, A.; Gupta, V. Methods for the Determination of Limit of Detection and Limit of Quantitation of the Analytical Methods. *Chronicles of Young Scientists* **2011**, *2*, 21.
(50) Asadpour-Zeynali, K.; Mollarasouli, F. Novel Electrochemical Biosensor Based on PVP Capped CoFe2O4@ CdSe Core-Shell Nanoparticles Modified Electrode for Ultra-Trace Level Determination of Rifampicin by Square Wave Adsorptive Stripping Voltammetry. *Biosens. Bioelectron.* **2017**, *92*, 509−516.
(51) Probes, M. *LIVE/DEAD BacLight Bacterial Viability Kit (L7012), Instruction Manual with Appendix*; Molecular Probes. Inc.; Eugene, Oreg, 1994.
(52) Ivanova, E. P.; Hasan, J.; Webb, H. K.; Gervinskas, G.; Juodkazis, S.; Truong, V. K.; Wu, A. H.; Lamb, R. N.; Baulin, V. A.; Watson, G. S. Bactericidal Activity of Black Silicon. *Nat. Commun.* **2013**, *4*, 2838.
(53) Park, H. M. *Comparing Group Means: T-Tests and One-Way ANOVA Using Stata, SAS, R, and SPSS*, 2009.
(54) Traunspurger, W.; Bergtold, M.; Goedkoop, W. The Effects of Nematodes on Bacterial Activity and Abundance in a Freshwater Sediment. *Oecologia* **1997**, *112*, 118−122.
(55) Masigol, M.; Barua, N.; Retterer, S. T.; Lokitz, B. S.; Hansen, R. R. Chemical Copatterning Strategies using Azlactone-Based Block Copolymers. *J. Vac. Sci. Technol., B: Nanotechnol. Microelectron.: Mater., Process., Meas., Phenom.* **2017**, *35*, 06GJ01.

DOI: 10.1021/acs.biomac.9b00609
Biomacromolecules XXXX, XXX, XXX−XXX

(56) Masigol, M.; Barua, N.; Lokitz, B. S.; Hansen, R. R. Fabricating Reactive Surfaces with Brush-Like and Crosslinked Films of Azlactone-Functionalized Block Co-Polymers. *J. Visualized Exp.* **2018**, *136*, No. e57562.
(57) Carter, M. C. D.; Lynn, D. M. Covalently Crosslinked and Physically Stable Polymer Coatings with Chemically Labile and Dynamic Surface Features Fabricated by Treatment of Azlactone-Containing Multilayers with Alcohol-, Thiol-, and Hydrazine-Based Nucleophiles. *Chem. Mater.* **2016**, *28*, 5063−5072.
(58) Catrouillet, S.; Fonteneau, C.; Bouteiller, L.; Delorme, N.; Nicol, E.; Nicolai, T.; Pensec, S.; Colombani, O. Competition between Steric Hindrance and Hydrogen Bonding in the Formation of Supramolecular Bottle Brush Polymers. *Macromolecules* **2013**, *46*, 7911−7919.
(59) Han, Y.; Cui, J.; Jin, J.; Jiang, W. Hydrogen Bonding Induced Protein Adsorption on Polymer Brushes: A Monte Carlo Study. *J. Mater. Chem. B* **2017**, *5*, 8479−8486.
(60) Ruckenstein, E.; Li, B. Steric Interactions between Two Grafted Polymer Brushes. *J. Chem. Phys.* **1997**, *107*, 932−942.
(61) Aden, B.; Street, D. P.; Hopkins, B. W.; Lokitz, B. S.; Kilbey, S. M. Tailoring Surface Properties through in Situ Functionality Gradients in Reactively Modified Poly(2-vinyl-4,4-dimethyl azlactone) Thin Films. *Langmuir* **2018**, *34*, 5204−5213.
(62) Li, Z.; Fu, Y.; Fang, W.; Li, Y. Electrochemical Impedance Immunosensor Based on Self-Assembled Monolayers for Rapid Detection of Escherichia coli O157:H7 with Signal Amplification Using Lectin. *Sensors* **2015**, *15*, 19212−19224.
(63) Mikaelyan, M. V.; Poghosyan, G. G.; Hendrickson, O. D.; Dzantiev, B. B.; Gasparyan, V. K. Wheat germ agglutinin and Lens culinaris agglutinin sensitized anisotropic silver nanoparticles in detection of bacteria: A simple photometric assay. *Anal. Chim. Acta* **2017**, *981*, 80−85.
(64) Kirkeby, S.; Friis, M.; Mikkelsen, H. B.; Cayé-Thomasen, P. Bacterial Adherence in Otitis Media: Determination of N-Acetylgalactosamine (GalNAc) Residues in the Submucosal Glands and Surface Epithelium of the Normal and Diseased Eustachian Tube. *Microb. Pathog.* **2011**, *51*, 48−57.
(65) Ajish, J. K.; Ajish Kumar, K. S.; Ruhela, A.; Subramanian, M.; Ballal, A. D.; Kumar, M. AIE based fluorescent self assembled glycoacrylamides for E.coli detection and cell imaging. *Sens. Actuators, B* **2018**, *255*, 1726−1734.
(66) Skoog, B.; Wichman, A. Calculation of the Isoelectric Points of Polypeptides from the Amino Acid Composition. *TrAC, Trends Anal. Chem.* **1986**, *5*, 82−83.
(67) Hu, S.; Wong, D. T. Lectin Microarray. *PROTEOMICS−Clinical Applications* **2009**, *3*, 148−154.
(68) Mandenius, C.-F.; Wang, R.; Aldén, A.; Bergström, G.; Thébault, S.; Lutsch, C.; Ohlson, S. Monitoring of Influenza Virus Hemagglutinin in Process Samples using Weak Affinity Ligands and Surface Plasmon Resonance. *Anal. Chim. Acta* **2008**, *623*, 66−75.
(69) Hsu, K.-L.; Mahal, L. K. A Lectin Microarray Approach for the Rapid Analysis of Bacterial Glycans. *Nat. Protoc.* **2006**, *1*, 543.
(70) Jalali, M.; AbdelFatah, T.; Mahshid, S. S.; Labib, M.; Sudalaiyadum Perumal, A.; Mahshid, S. A Hierarchical 3D Nano-structured Microfluidic Device for Sensitive Detection of Pathogenic Bacteria. *Small* **2018**, *14*, 1801893.
(71) Wang, S.; Wang, H.; Jiao, J.; Chen, K.-J.; Owens, G. E.; Kamei, K.-i.; Sun, J.; Sherman, D. J.; Behrenbruch, C. P.; Wu, H.; Tseng, H.-R. Three-Dimensional Nanostructured Substrates toward Efficient Capture of Circulating Tumor Cells. *Angew. Chem.* **2009**, *121*, 9132−9135.
(72) Chen, W.; Weng, S.; Zhang, F.; Allen, S.; Li, X.; Bao, L.; Lam, R. H. W.; Macoska, J. A.; Merajver, S. D.; Fu, J. Nanoroughened Surfaces for Efficient Capture of Circulating Tumor Cells without using Capture Antibodies. *ACS Nano* **2012**, *7*, 566−575.
(73) Toze, S. PCR and the Detection of Microbial Pathogens in Water and Wastewater. *Water Res.* **1999**, *33*, 3545−3556.
(74) Francy, D. S.; Stelzer, E. A.; Bushon, R. N.; Brady, A. M.; Mailot, B. E.; Spencer, S. K.; Borchardt, M. A.; Elber, A. G.; Riddell, K. R.; Gellner, T. M. Quantifying Viruses and Bacteria in Wastewater—results, Interpretation Methods, and Quality Control. *US Geological Survey Scientific Investigations Report*, 2011; p 5150.
(75) Groen, J.; Pannek, J.; Castro Diaz, D.; Del Popolo, G.; Gross, T.; Hamid, R.; Karsenty, G.; Kessler, T. M.; Schneider, M.; Blok, B. Summary of European Association of Urology (EAU) Guidelines on Neuro-Urology. *Eur. Urol.* **2016**, *69*, 324−333.
(76) Puttaswamy, S.; Lee, B. D.; Sengupta, S. Novel Electrical Method for Early Detection of Viable Bacteria in Blood Cultures. *J. Clin. Microbiol.* **2011**, *49*, 2286−2289.
(77) Yagupsky, P.; Nolte, F. S. Quantitative Aspects of Septicemia. *Clin. Microbiol. Rev.* **1990**, *3*, 269−279.
(78) Lin, N.; Berton, P.; Moraes, C.; Rogers, R. D.; Tufenkji, N. Nanodarts, Nanoblades, and Nanospikes: Mechano-Bactericidal Nanostructures and Where to Find Them. *Adv. Colloid Interface Sci.* **2018**, *252*, 55−68.
(79) Thompson, M. A.; Onyeziri, M. C.; Fuqua, C. Function and Regulation of Agrobacterium Tumefaciens Cell Surface Structures that Promote Attachment. *Curr. Top. Microbiol. Immunol.* **2018**, *418*, 143−184.
(80) Li, G.; Brown, P. J. B.; Tang, J. X.; Xu, J.; Quardokus, E. M.; Fuqua, C.; Brun, Y. V. Surface contact stimulates the just-in-time deployment of bacterial adhesins. *Mol. Microbiol.* **2012**, *83*, 41−51.
(81) Tsang, P. H.; Li, G.; Brun, Y. V.; Freund, L. B.; Tang, J. X. Adhesion of Single Bacterial Cells in the Micronewton Range. *Proc. Natl. Acad. Sci. U.S.A.* **2006**, *103*, 5764−5768.
(82) Merritt, P. M.; Danhorn, T.; Fuqua, C. Motility and Chemotaxis in Agrobacterium Tumefaciens Surface Attachment and Biofilm Formation. *J. Bacteriol.* **2007**, *189*, 8005−8014.
(83) Liu, X.; Lei, Z.; Liu, F.; Liu, D.; Wang, Z. Fabricating Three-Dimensional Carbohydrate Hydrogel Microarray for Lectin-Mediated Bacterium Capturing. *Biosens. Bioelectron.* **2014**, *58*, 92−100.

DOI: 10.1021/acs.biomac.9b00609
Biomacromolecules XXXX, XXX, XXX−XXX